Structural Elucidation of Light Activated Vesicles

ARTICLE *in* JOURNAL OF PHYSICAL CHEMISTRY LETTERS · FEBRUARY 2010

Impact Factor: 7.46 · DOI: 10.1021/jz100226v

THE JOURNAL OF PHYSICAL CHEMISTRY Letters

pubs.acs.org/JPCL

Structural Elucidation of Light Activated Vesicles

Anan Yaghmur,*[,†] Lauri Paasonen,[†,§] Marjo Yliperttula,[§] Arto Urtti,[†] and Michael Rappolt*[,∥]

[†]Faculty of Pharmaceutical Sciences, Department of Pharmaceutics and Analytical Chemistry, University of Copenhagen, Copenhagen, Denmark, [†]Centre for Drug Research, University of Helsinki, Helsinki, Finland, [§]Division of Biopharmacy and Pharmacokinetics, Faculty of Pharmacy, University of Helsinki, Helsinki, Finland, and [∥]Institute of Biophysics and Nanosystems Research (IBN), Austrian Academy of Sciences, Graz, Austria

ABSTRACT In the present study, synchrotron small-angle X-ray scattering (SAXS) combined with a UV light source (in situ SAXS-UV irradiation) was used to determine the structure response of gold nanoparticle (NP)-loaded vesicles. The investigated system consisted of multilamellar vesicles of N-methylated dioleoylphosphatidylethanolamine (DOPE-Me) containing hydrophilic gold NPs with a size of 40 Å. Our results indicate drastic optothermically induced structural changes in these gold NP-loaded aqueous dispersions, which are accompanied by strong alterations in the phospholipid membrane permeability. A structural mechanism from well-ordered multilamellar vesicles in the fluid lamellar (L_α) phase to an inverted type hexagonal liquid crystalline (H_2) phase via the formation of an intermediate phase of uncorrelated fluid bilayers is proposed. In general, these investigations are also crucial for the understanding of the potential of gold NP-loaded model phospholipid systems as efficient drug nanocarriers aiming to improve drug targeting and releasing on demand.

SECTION Biophysical Chemistry

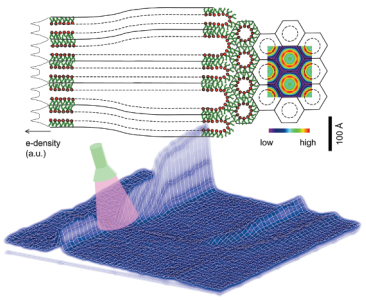

Stimulus-responsive nanomaterials have attracted increasing interest owing to their potential applications in the formation of drug nanocarriers for targeting and controlling drug release.[1−8] A promising approach is based on using temperature-sensitive gold nanoparticle (NP)-loaded liposomes that can release drug content on demand at a specific administration site and within a controllable time of heating or light exposure by enhancing the permeability of phospholipid membranes.[1,9] These liposomes respond to an external stimulus such as UV or near-infrared (NIR) pulsed laser and enable the occurrence of light-induced "hot spots of NPs" and simultaneously induce heat transfer to the surrounding lipid/water bilayers.[1,4,10] In a recent work, Paasonen et al.[1] demonstrated that gold NP-loaded liposomes based on a binary lipid mixture of dipalmitoylphosphatidylcholine (DPPC) and distearoylphosphatidylcholine (DSPC) induce light-triggered contents release above body temperature as exposed to UV light. In response to light irradiation, the leakage of these liposomes is attained through melting the lipid bilayers near the main transition temperature (structural transition from gel to fluid liquid crystalline phase).

In general, temperature-induced lamellar−nonlamellar transitions upon heating lipid systems could also provide attractive drug nanocarriers that enable releasing solubilized drug content on demand. In literature, these transitions have attracted increasing interest owing to their vital role in modulating membrane fusion and fat digestion in biological cells.[11−18] In this context, heat-sensitive gold NP-loaded liposomal formulations with light-induced lamellar−nonlamellar transition above the body temperature also have potential in the development of stimulus-responsive nanocarriers. It is clear that the optimal utilization of these lipid systems requires elucidating the light-induced structural changes.

In the present study, our main goal is to shed light onto the impact of UV light exposure on aqueous dispersions of N-methylated dioleoylphosphatidylethanolamine (DOPE-Me), which have often been chosen as a model system because the involved phase transitions are particularly sensitive to the presence of agents that promote or inhibit membrane fusion.[13,19−21] In our study, carrying out experiments with synchrotron small-angle X-ray scattering in the presence of UV light source (in situ SAXS-UV irradiation) is used for checking the possible enhancement of membrane fusion and also for providing more details on light-induced structural transitions. We believe that these investigations in the future will allow controlling such systems and optimizing their properties.

To characterize in detail the light-responsive nanostructures of the gold NP-loaded DOPE-Me aqueous dispersions and to estimate the final sample temperature after light activation, three different time-resolved experiments were performed. Figure 1 shows examples of the light-induced structural transitions observed in the gold NP-loaded DOPE-Me at different heating conditions. In panel a, the final temperature, T_f, was lower than the H_2 phase formation temperature, T_H ($T_f \sim 59$ °C); in panel b, T_f was greater than T_H ($T_f \sim 77$ °C;

Received Date: February 18, 2010
Accepted Date: February 23, 2010
Published on Web Date: February 26, 2010

DOI: 10.1021/jz100226v | J. Phys. Chem. Lett. 2010, 1, 962–966

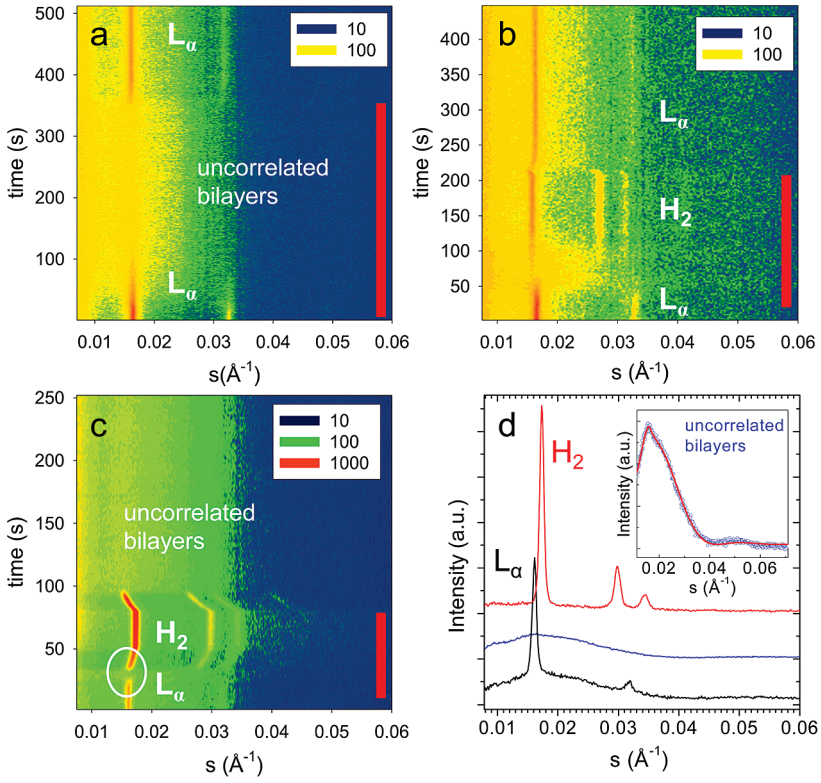

Figure 1. Time-resolved SAXS experiments on hydrophilic gold NP-loaded liposomes. (a) During UV-light heating (marked by a red bar), disorder is induced in the liposomes. (b) Heating above T_H, the H_2 phase forms via a disordered L_α phase. (c) After superheating the sample, only uncorrelated bilayers remain. In panels a−c, the X-ray intensities are color coded in the insets, and the transition to H_2 phase in panel c is highlighted in white. (d) Typical diffraction patterns just before, during, and after the L_α−H_2 transition are shown. The blue curve shows the disordered phase consisting of mainly uncorrelated bilayers, and the inset displays the global fitting (red line) of this intermediate phase considering both the form and the structure factor contributions (for details, see the Supporting Information).

T_H = 71 °C); and in panel c, the sample was superheated ($T_f \sim 106$ °C). Before the UV-light was switched on, the sample temperature was 25 °C, and the diffraction patterns display the first- and second-order Bragg-peaks of well ordered multilamellar vesicles in the fluid L_α phase. Apart from an increased scattering contribution in the low angle regime, no further differences are observed with respect to the nonloaded vesicles. The position and the Bragg-peak intensities remain the same, i.e., the presence of the gold NPs do not alter the composition of the multilamellar vesicles (see also the Supporting Information). Therefore, the gold NPs are likely to absorb, in part, at the outer surface of the vesicles, and some amount is expected to be in the surrounding excess water.

After switching on the UV light, the first induced phase is still composed of fluid bilayers, but without positional correlation. Here, the SAXS patterns mainly display diffuse scattering, i.e., to a great extent the form factor contribution of the bilayer. However, global analysis of this data as described in the Supporting Information reveal that not all lamellae converted to an unbound state, but a few percent of the oligolamellar membrane stacks remain (cf. to inset of Figure 1d and the Supporting Information).

The time for formation of this intermediate phase depends on the final temperature and takes about 90 s for $T_f \sim 59$ °C (Figure 1a), 35 s for $T_f \sim 77$ °C (Figure 1b), and only 5 s for $T_f \sim 106$ °C (Figure 1c). Above the transition temperature, T_H, finally the H_2 phase forms (panels b and c). This is most clearly seen in panel c (highlighted in white): the real-time evolution of the SAXS patterns demonstrates the drastic impact of UV light on the curvature of DOPE-Me monolayers. Illumination with the UV light source quickly leads to a significant effect on the lamellar (L_α) phase: it induces within a few seconds a disordered bilayer phase, and shortly thereafter the H_2 phase. One minute after switching off the light, the nanostructure retransforms to a vesicular dispersion from the H_2 phase with a SAXS pattern that is mainly dominated by diffuse scattering. Interestingly, the heating process is not reversible in the case of superheating. The sample does not reorganize into well-ordered multilamellar vesicles as seen during passive cooling in Figure 1a,b, but remains in the disordered state. The most probable explanation would be that, under these extreme conditions, unilamellar vesicles are formed. Further details on the temporal evolution of different lattice spacings can be studied in the Supporting Information.

The L_α−H_2 structural transition has been explained by a variety of models; especially different mechanisms were proposed for phosphatidylethanolamine (PE)/water model systems (see ref 22 and the references therein). Unfortunately, several of these models suffer from incorrect geometrical dimensions, such as unrealistically bent monolayers or water layers that are too thick. The most common reason for this lies in the lack of detailed structural information. Part of

DOI: 10.1021/jz100226v | J. Phys. Chem. Lett. 2010, 1, 962–966

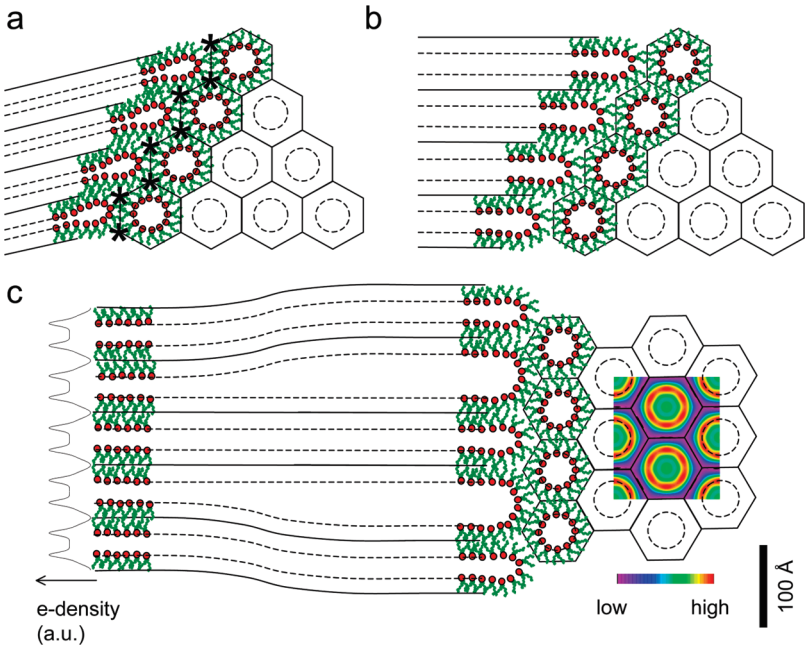

Figure 2. Interface reconstruction involving the L_α and the H_2 phases. For clarity, lipid molecules are superimposed to the outlined locations of the polar interfaces (dashed lines) and the methyl trough regions (full lines). (a) Interface model deduced from electron density maps of POPE (T_H = 74 °C). (b) Coplanar interface model reconstructed on the basis of electron density maps of DOPE-Me data (T_H = 71 °C). (c) Order−disorder−order model depicted for the DOPE-Me system. The electron density profile of the L_α phase is shown at the far left of panel c, and the electron density map of the H_2 phase is shown on the far right of c. For the H_2 phase, the electron density values are color coded.

the motivation for this work was to use SAXS at a high brilliance synchrotron source to address this deficiency for DOPE-Me aqueous dispersion. Recently, this strategy has led to the first detailed interface reconstruction involving the L_α and H_2 phases in palmitoyl-oleoyl-phosphatidylethanolamine (POPE) water systems[22] (Figure 2a). In contrast to N-methylated PEs, long-chain PE/water systems display a long-range coexistence region of both involved phases.[22]

In this respect, it is important to note that no disordered phase is spotted during the transition process. Therefore Laggner and Kriechbaum[23] adopted the model of a diffusion-free martensitic process, in which the two neighboring lattices are mutually inclined. In this way, the path length of rearranging lipid molecules in the interface region is minimized. This view is depicted in a refined manner in Figure 2a. It should be noted that the bulb-like form of bent back monolayers is a consequence of the stringent constraint to minimize the interstitial regions of the interface (*). Free energy simulations in the transition regime of POPE have confirmed that this bulb-like form of monolayers is the energetically most favorable.[24]

Figure 2b illustrates the same transition model for the geometry of the DOPE-Me system investigated here. Although the resulting snapshot of the interface looks quite appealing, it does not account for the disordered phase observed in the SAXS study. According to this model, the arrangement is coplanar, i.e., the repeat distance of the L_α phase and the d_{10}-spacing of the H_2 phase have an epitaxial relation. On the contrary, our SAXS results show that the transition mechanism proceeds via an intermediate disordered phase. Such an order−disorder−order transition model is shown in Figure 2c. On the left-hand side, the L_α phase is reconstructed on the basis of the determined electron density profile at 71 °C, and on the right-hand side the H_2 phase is illustrated according to the electron density map determined just above 71 °C (for structural details see the Supporting Information). Importantly, when the initial and the final lattices are not oriented in a coplanar manner, the lattice repeat distance of the L_α phase can not be retained. It is worth noting that, even if two neighboring bilayers remain in the bound state (L_α membrane−membrane distance is conserved), simultaneously the next-nearest lamellae is disturbed to adhere at the preferred distance. This is exactly what we observe (see Figure 1d, inset): the disordered phase consists of mainly uncorrelated bilayers coexisting with very few bound membranes (global fitting reveals 5 ± 3 correlated bilayers; see Supporting Information). The reason why the transition favors to proceed via a disordered intermediate lamellar phase is twofold. First, the DOPE-Me bilayers are not as strongly bound as in the pure PE/water systems (the interlamellar distance, $d_{W(DOPE\text{-}Me)}$ = 19 Å at 71 °C and $d_{W(POPE)}$ = 5 Å (ref 22) at 74 °C, respectively), and second, the concentration of water in the L_α phase is too high to allow an ordered transition without massive diffusion of the surplus water molecules. The number of water molecules per lipid, n_W, reduces by about 50% during the L_α−H_2 transition (n_{Wlam} = 29 and n_{Whex} = 19), which means that the surrounding disordered lamellar phase (and excess of water regions) have to take up 10 water molecules for every lipid molecule that rearranges in the H_2 phase (see Supporting Information). An alternative

DOI: 10.1021/jz100226v | J. Phys. Chem. Lett. 2010, 1, 962–966

transformation pathway from flat bilayers into hexagonally packed monolayer cylinders is believed to involve complex structural rearrangements including the aggregation of trans-monolayer contacts into a body-centered cubic or primitive tetragonal phase, which in turn serves as a precursor for the formation of the H_2 phase.[11,12] However, such three-dimensional (3D) intermediate phase was not observed in our study.

In summary, the absorption of UV light by the gold NPs triggers fast $L_\alpha - H_2$ structural transition in the DOPE-Me aqueous dispersions. This significant UV-activated impact on the membrane permeability can be utilized for the formation of stimulus-responsive systems and drug nanocarriers with controlled drug release.

EXPERIMENTAL METHODS

Sample Preparation. DOPE-Me was purchased from Avanti Polar Lipids (Alabasta, LA) and dissolved in chloroform. This solvent was then evaporated using a gentle stream of nitrogen, followed by drying under vacuum for at least 12 h in order to completely remove the residual organic solvent. The dry lipid film was hydrated by adding an aqueous stock solution[1] of hydrophilic gold NPs containing 1 mg NPs/mL and having an average NP size of 40 Å, carrying out at least five freeze−thaw cycles between liquid nitrogen and room temperature, and then homogenizing several times during the thawing steps by vigorous vortexing. The used gold NPs were synthesized as previously described,[1] and the liposomal samples were formed with a fixed total lipid concentration of 10 wt %.

Combined Synchrotron SAXS and UV-Light Set-Up. Synchrotron SAXS patterns were recorded at the Austrian SAXS beamline[25] (camera length 75 cm) at the synchrotron light source ELETTRA (Trieste, Italy) using a one-dimensional position sensitive detector (Gabriel type), which covered the s-range ($s = 2 \sin\theta/\lambda$, where λ is the wavelength and 2θ is the scattering angle) of interest from about 1/640 to 1/13 $Å^{-1}$ at an X-ray energy of 8 keV. Silver behenate ($CH_3-(CH_2)_{20}-COOAg$ with a d-spacing value of 58.38 Å) was used as a standard to calibrate the angular scale of the measured intensity.[26] In the absence of gold NPs, the control sample was sealed in a thin-walled quartz capillary (Anton-Paar, Graz, Austria) and thermostatted with a programmable water bath (stability ± 0.1 °C, Unistat CC, Huber, Offenburg, Germany). Before each time-resolved experiment, fresh sample was filled into the capillary, and static measurements were done at 25 °C with an exposure time of 30 s. The exposure time during the UV-light experiments was 2 s for each frame. The temperature scan on pure DOPE-Me was performed at a scan rate of 1 °C/min. Two X-ray patterns were recorded per minute with a constant exposure time of 10 s. Between each exposure, a small solenoid driven shutter blocked the direct X-ray beam in order to minimize the total radiation dosage on the sample. The SAXS analysis and electron density calculations are given in the Supporting Information.

UV irradiation of DOPE-Me aqueous dispersions was done at a wavelength of 365 nm with an EXFO Omnicure S1000 light source (EXFO Life Sciences and Industrial Division, Ontario, Canada). The light source was operated with an external switch, a 365 nm filter, a 5 mm optical guide, and an adjustable collimator. The distance from the collimator lens to the sample capillary was 40, 50, and 62 mm, respectively.

SUPPORTING INFORMATION AVAILABLE SAXS analysis, electron density calculations, and supporting figures. This material is available free of charge via Internet at http://pubs.acs.org.

AUTHOR INFORMATION

Corresponding Author:

*To whom correspondence should be addressed. Tel.: +45 35 33 65 41. Fax: +45 35336030. E-mail: aya@farma.ku.dk (A.Y.); michael.rappolt@oeaw.ac.at (M.R.).

REFERENCES

(1) Paasonen, L.; Laaksonen, T.; Johans, C.; Yliperttula, M.; Kontturi, K.; Urtti, A. Gold Nanoparticles Enable Selective Light-Induced Contents Release from Liposomes. *J. Controlled Release* **2007,** *122*, 86–93.
(2) Yliperttula, M.; Chung, B. G.; Navaladi, A.; Manbachi, A.; Urtti, A. High-Throughput Screening of Cell Responses to Biomaterials. *Eur. J. Pharm. Sci.* **2008,** *35*, 151–160.
(3) Li, J.; Wang, B. C.; Wang, Y. Z.; Liu, P.; Qiao, W. L. Preparation and Characterization of Thermosensitive Nanoparticles for Targeted Drug Delivery. *J. Macromol. Sci., Part A: Pure Appl. Chem.* **2008,** *45*, 833–838.
(4) Wu, G. H.; Milkhailovsky, A.; Khant, H. A.; Fu, C.; Chiu, W.; Zasadzinski, J. A. Remotely Triggered Liposome Release by Near-Infrared Light Absorption via Hollow Gold Nanoshells. *J. Am. Chem. Soc.* **2008,** *130*, 8175–8177.
(5) del Amo, E. M.; Urtti, A. Current and Future Ophthalmic Drug Delivery Systems. A Shift to the Posterior Segment. *Drug Discovery Today* **2008,** *13*, 135–143.
(6) Lu, J.; Choi, E.; Tamanoi, F.; Zink, J. I. Light-Activated Nanoimpeller-Controlled Drug Release in Cancer Cells. *Small* **2008,** *4*, 421–426.
(7) Fong, W. K.; Hanley, T.; Boyd, B. J. Stimuli Responsive Liquid Crystals Provide 'On-Demand' Drug Delivery In Vitro and In Vivo. *J. Controlled Release* **2009,** *135*, 218–226.
(8) Robbins, G. P.; Jimbo, M.; Swift, J.; Therien, M. J.; Hammer, D. A.; Dmochowski, I. J. Photoinitiated Destruction of Composite Porphyrin−Protein Polymersomes. *J. Am. Chem. Soc.* **2009,** *131*, 3872–3874.
(9) Kojima, C.; Hirano, Y.; Yuba, E.; Harada, A.; Kono, K. Preparation and Characterization of Complexes of Liposomes with Gold Nanoparticles. *Colloids Surf. B* **2008,** *66*, 246–252.
(10) Richardson, H. H.; Carlson, M. T.; Tandler, P. J.; Hernandez, P.; Govorov, A. O. Experimental and Theoretical Studies of Light-to-Heat Conversion and Collective Heating Effects in Metal Nanoparticle Solutions. *Nano Lett.* **2009,** *9*, 1139–1146.
(11) Siegel, D. P. The Modified Stalk Mechanism of Lamellar/Inverted Phase Transitions and Its Implications for Membrane Fusion. *Biophys. J.* **1999,** *76*, 291–313.
(12) Siegel, D. P.; Epand, R. M. The Mechanism of Lamellar-to-Inverted Hexagonal Phase Transitions in Phosphatidylethanolamine: Implications for Membrane Fusion Mechanisms. *Biophys. J.* **1997,** *73*, 3089–3111.
(13) Harroun, T. A.; Balali-Mood, K.; Gourlay, I.; Bradshaw, J. P. The Fusion Peptide of Simian Immunodeficiency Virus and the Phase Behaviour of N-Methylated Dioleoylphosphatidylethanolamine. *Biochim. Biophys. Acta* **2003,** *1617*, 62–68.

DOI: 10.1021/jz100226v | *J. Phys. Chem. Lett.* **2010,** *1*, 962–966

(14) Yaghmur, A.; Laggner, P.; Sartori, B.; Rappolt, M. Calcium Triggered $L_\alpha-H_2$ Phase Transition Monitored by Combined Rapid Mixing and Time-Resolved Synchrotron SAXS. *PLoS ONE* **2008,** *3*, e2072.
(15) Gruner, S. M.; Tate, M. W.; Kirk, G. L.; So, P. T.; Turner, D. C.; Keane, D. T.; Tilcock, C. P.; Cullis, P. R. X-Ray Diffraction Study of the Polymorphic Behavior of N-Methylated Dioleoylphosphatidylethanolamine. *Biochemistry* **1988,** *27*, 2853–2866.
(16) Patton, J. S.; Carey, M. C. Watching Fat Digestion. *Science* **1979,** *204*, 145–148.
(17) Hui, S. W.; Stewart, T. P.; Boni, L. T.; Yeagle, P. L. Membrane Fusion Through Point Defects in Bilayers. *Science* **1981,** *212*, 921–923.
(18) Yaghmur, A.; Laggner, P.; Almgren, M.; Rappolt, M. Self-Assembly in Monoelaidin Aqueous Dispersions: Direct Vesicles to Cubosomes Transition. *PLoS ONE* **2008,** *3*, e3747.
(19) Siegel, D. P.; Banschbach, J.; Alford, D.; Ellens, H.; Lis, L. J.; Quinn, P. J.; Yeagle, P. L.; Bentz, J. Physiological Levels of Diacylglycerols in Phospholipid Membranes Induce Membrane Fusion and Stabilize Inverted Phases. *Biochemistry* **1989,** *28*, 3703–3709.
(20) Siegel, D. P.; Cherezov, V.; Greathouse, D. V.; Koeppe, R. E.; Killian, J. A.; Caffrey, M. Transmembrane Peptides Stabilize Inverted Cubic Phases in A Biphasic Length-Dependent Manner: Implications for Protein-Induced Membrane Fusion. *Biophys. J.* **2006,** *90*, 200–211.
(21) Cherezov, V.; Siegel, D. P.; Shaw, W.; Burgess, S. W.; Caffrey, M. The Kinetics of Non-lamellar Phase Formation in DOPE-Me: Relevance to Biomembrane Fusion. *J. Membr. Biol.* **2003,** *195*, 165–182.
(22) Rappolt, M.; Hickel, A.; Bringezu, F.; Lohner, K. Mechanism of the Lamellar/Inverse Hexagonal Phase Transition Examined by High Resolution X-Ray Diffraction. *Biophys. J.* **2003,** *84*, 3111–3122.
(23) Laggner, P.; Kriechbaum, M. Phospholipid Phase Transitions: Kinetics and Structural Mechanisms. *Chem. Phys. Lipids* **1991,** *57*, 121–145.
(24) Mares, T.; Daniel, M.; Perutkova, S.; Perne, A.; Dolinar, G.; Iglic, A.; Rappolt, M.; Kralj-Iglic, V. Role of Phospholipid Asymmetry in the Stability of Inverted Hexagonal Mesoscopic Phases. *J. Phys. Chem. B* **2008,** *112*, 16575–16584.
(25) Amenitsch, H.; Rappolt, M.; Kriechbaum, M.; Mio, H. L. P.; et al. First Performance Assessment of the Small-Angle X-Ray Scattering Beamline at ELETTRA. *J. Synchrotron Rad.* **1998,** *5*, 506–508.
(26) Huang, T. C.; Toraya, H.; Blanton, T. N.; Wu, Y. X-Ray-Powder Diffraction Analysis of Silver Behenate, A Possible Low-Angle Diffraction Standard. *J. Appl. Crystallogr.* **1993,** *26*, 180–184.

DOI: 10.1021/jz100226v | *J. Phys. Chem. Lett.* **2010,** *1*, 962–966

Supporting Information

Structural Elucidation of Light Activated Vesicles

Anan Yaghmur[*,‡], *Lauri Paasonen*[†], *Marjo Yliperttula*[⊥], *Arto Urtti*[†], *Michael Rappolt*[*,§]

[‡]Faculty of Pharmaceutical Sciences, Department of Pharmaceutics and Analytical Chemistry, University of Copenhagen, Copenhagen, Denmark

[†]Centre for Drug Research, University of Helsinki, Helsinki, Finland

[⊥]Division of Biopharmacy and Pharmacokinetics, Faculty of Pharmacy, University of Helsinki, Helsinki, Finland

[§]Istitute of Biophysics and Nanosystems Research (IBN), Austrian Academy of Sciences, Graz, Austria

Received date

E-mail: aya@farma.ku.dk; michael.rappolt@oeaw.ac.at

SAXS Analysis and Electron Density Calculations

The two dimensional (2D) electron density map of the H_2-phase of DOPE-Me/water at 74.5 °C was derived from the SAXS diffraction pattern by standard procedures (for details see Rappolt et al.[1]). After the raw data had been corrected for detector efficiency, and the background scattering both from water and the sample cell had been subtracted, all Bragg peaks were fitted by Lorentzian distributions. The fittings were carried out with the software package Origin 5.0 (Microcal Software). Next the intensities were also corrected for their multiplicity, i.e. the intensity of the (2,1) peaks was divided by 2. Thereafter, a Lorentz correction was applied to all powder diffraction images by multiplying each peak intensity (peak area) by its corresponding wave vector s^2 (for discussion of the Lorentz correction on powder samples, the interested reader is directed to ref[2]). Finally, the square root of the corrected peak intensity determined the form factor, F, of each respective reflection. The electron density contrast was calculated by the Fourier synthesis. The phase combination (+1;-1;-1;+1;+1) for the reflections (10), (11), (20), (21) and (30) was taken from literature[3]. Table S1 shows the structural parameters of the H_2 phase of DOPE-Me based aqueous dispersion at 74.5 °C. One static scattering pattern of the uncorrelated bilayers recorded at 71 °C was analyzed by the global analysis program (GAP). This model uses one Gaussian for the headgroups and another for the hydrophobic core. A more detailed description of this model is given elsewhere[4,5]. The fit parameters derived from the GAP evaluation for these uncorrelated bilayers (Figure 1d, inset) are presented in Table S2. In Table S3, the calculated properties of the fully hydrated DOPE-Me phases at a temperature, which is very close to the L_α/H_2 transition temperature (T_H = 71 °C), are shown.

Supporting Experimental Details

Figure S1 compares the raw diffraction data of DOPE-ME dispersions with and without loaded hydrophilic gold nanoparticles (NPs). The d-spacings of the fluid L_α phase and the intensities are within

experimental errors the same. At 25 °C, both aqueous dispersions have *d* value of 61. 4 Å. This means that the NPs do not significantly alter the composition and the structure of the multilamellar vesicles.

Table S1. Structural parameters of the inverse hexagonal (H_2) phase of DOPE-Me based aqueous dispersion at 74.5 °C.

Parameter	Value
d_{hex} (Å)	75.2 (74.5 at 71 °C)
F_{10}	1.00
F_{11}	0.97
F_{20}	0.77
F_{21}	0.36
F_{30}	0.39
R_P (Å)	22.3 (~22.1[*] at 71 °C)
V_L (Å^3)	1220[§]

The unit cell spacing, d_{hex}, amplitudes of the reflections (1,0), (1,1), (2,0), (2,1) and (3,0), the distance from the centre of the rod to the phosphate group, R_P, and the volume of the lipid molecule, V_L, are given. [*]By interpolation estimated value of R_P at the transition temperature (T_H = 71 °C). [§]Lipid volume was taken from Gruner et al.[7].

These gold NPs having a diameter of ~ 40 Å are approximately twice as big as the free interlamellar water spacing, and since no structural perturbation can be seen, this implies that the gold NPs are likely to absorb, in part, at the outer surface of the vesicles and a considerable amount is expected to be in the

surrounding excess water. Further, significant gold scattering contributions are only observed in the low angle regime (red arrow in Figure S1), i.e. from the gold NPs themselves. Structure factor contributions arising from densely aggregating NPs are absent. These findings are confirmed by previous transmission electron microscopy measurements[6].

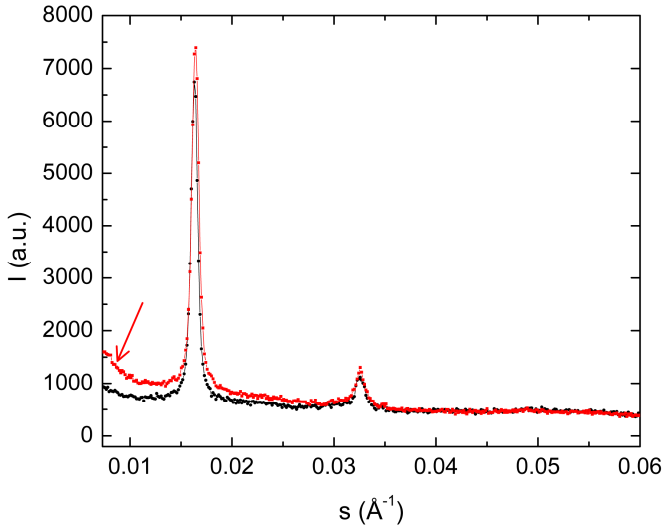

Figure S1. Raw X-ray diffraction data of DOPE-ME with gold NPs (red dots) and without (black dots). Apart from data normalization in the high *s*-regime no further data reduction was applied. The temperature was 25 °C and the red colored arrow indicates additional scattering arising from the gold NPs.

Figure S2a presents the time-resolved SAXS patterns of the gold NPs-free aqueous dispersion that is heated through the L_α/H_2 transition. Figure S2b shows the variation in the corresponding *d*-spacing of this dispersion as a function of temperature in our study and that reported previously by Gruner et al.[7]. It should be noted that our results do not show any indication on the formation of inverted type bicontinuous cubic phase (V_2) from the L_α phase. Siegel and coworkers[8-11] showed in previous reports that this fully hydrated phospholipid can form the V_2 within a temperature interval starting at

62 °C and thus can induce indirect L_α-H_2 transition as heating is done at slow scan rates or during prolonged incubations of months at temperatures below the L_α-H_2 transition temperature.

Table S2. Fit parameters derived from the GAP evaluation of the SAXS pattern (Figure 1d, inset) for the DOPE-Me based liposomes at 71 °C.

Parameter	Value
d (Å)	64.5 ± 0.8
N_{mean}	5 ± 3
η	1.4 ± 0.1
z_H (Å)	18.6 ± 0.5 (19.5[§] at 2 °C)
σ_H (Å)	3.0 ± 0.6
σ_C (Å)	6.6 ± 1.0
ρ_r	-0.99 ± 0.07
N_{diff}	0.93 ± 0.14

The parameters given are the d-spacing, the membrane correlation number, N_{mean}, the Caillé parameter, η, the headgroup position, z_H, the headgroup width, σ_H, the width of the hydrophobic core, σ_C, the relative electron density of the bilayer trough set in relation to the headgroup density, ρ_r, and the fraction of the diffuse scattering, N_{diff}. [§]Value published by Gruner et al.[7].

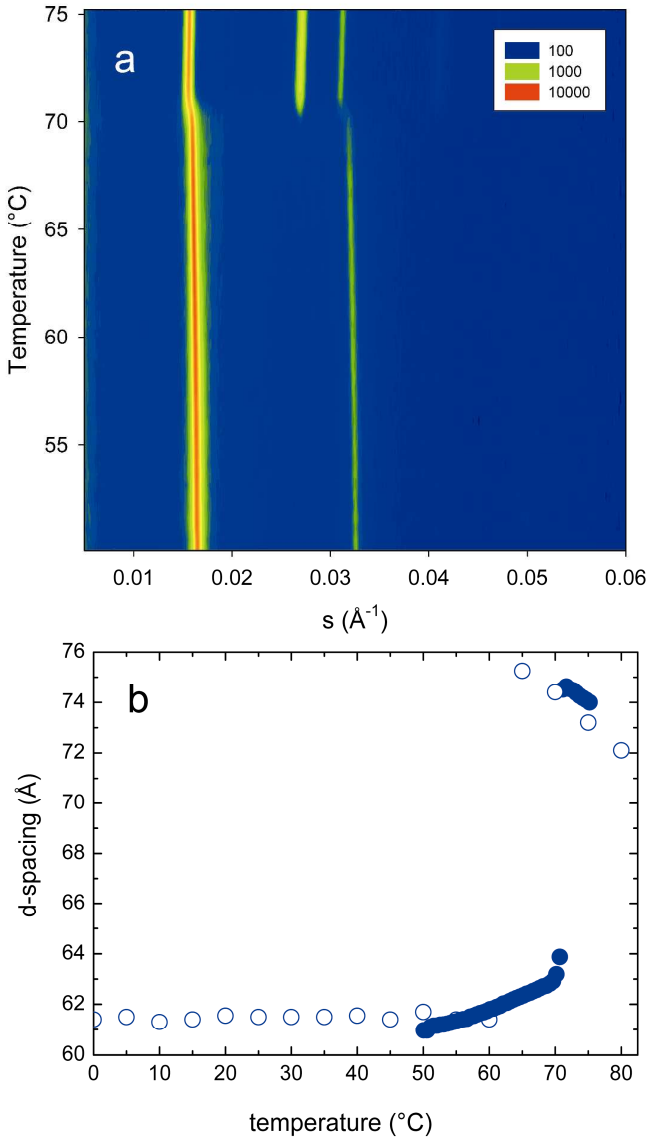

Figure S2. Time-resolved temperature scan on gold NPs-free DOPE-Me aqueous dispersion. Panel (a) displays the recorded raw SAXS data and panel (b) displays the corresponding *d*-spacings. Experimental data from Gruner et al.[7] is shown by open circles. In the temperature range of 50-71 °C, the lattice parameter of the formed multi-lamellar vesicles (MLVs) increases during heating from 61.0 to 64.5 Å. At 71 °C, the L_α-H_2 transition is observed. The lattice parameter of the newly formed H_2 phase decreases linearly with increasing temperature (d_{hex} (Å) = -0.1835 * T + 87.8, where d_{hex} is the lattice constant of the H_2 phase, and T is the investigated temperature).

Figure S3 illustrates the evolution of the lattice spacings during the time-resolved SAXS experiments on the gold NPs-loaded DOPE-ME liposomes (Figure S3a-c refers to Figure 1a-c). For these aqueous dispersions, the final sample temperature, T_f, was estimated from the lattice parameter of the H_2 phase at a lamp to sample distance of 50 mm (this experiment is illustrated in Figure 1b). The minimum lattice spacing reached was 73.6 Å (Figure S3b), which corresponds to a temperature of 77 °C (compare Figure S1b). From this value, it follows that the T_f at a distance of 62 mm (lamp distance in experiment of Figure 1a) is about 59 °C, and at sample to lamp distance of 40 mm (lamp distance in experiment of Figure 1c) the T_f equals about 106 °C. Since no signs of air bubbles were detected by SAXS in the latter case, the sample was most probably superheated under these extreme experimental conditions. In Figure S3c (referring to Figure 1c), the heating rate, $\Delta T/\Delta t$, can be estimated by taking a closer look to the variation of the lattice spacing of the H_2 phase with time in the interval of 30-50 s. In this case, the calculated $\Delta T/\Delta t$ value is approximately 60 °C/min. For the other two experiments, we accordingly estimated $\Delta T/\Delta t$ to be approximately 42 °C/min (lamp distance 50 mm, referring to Figure 1b) and 27 °C/min (lamp distance 62 mm, referring to Figure 1a)), respectively.

Table S3. Hydrational properties of the DOPE-Me phases at a temperature, which is very close to the L_α/H_2 transition temperature (T_H = 71 °C).

Parameter	Value
A_{lam} (Å^2)	65
A_{hex} (Å^2)	51
$V_{W\,lam}$ (Å^3)	880
$V_{W\,hex}$ (Å^3)	560
$n_{W\,lam}$	29
$n_{W\,hex}$	19

The headgroup area per lipid at the phosphate region, A, the water volume per lipid, V_W; and the number of waters per lipid, n_W, are determined after recipes given in Rappolt et al.[1].

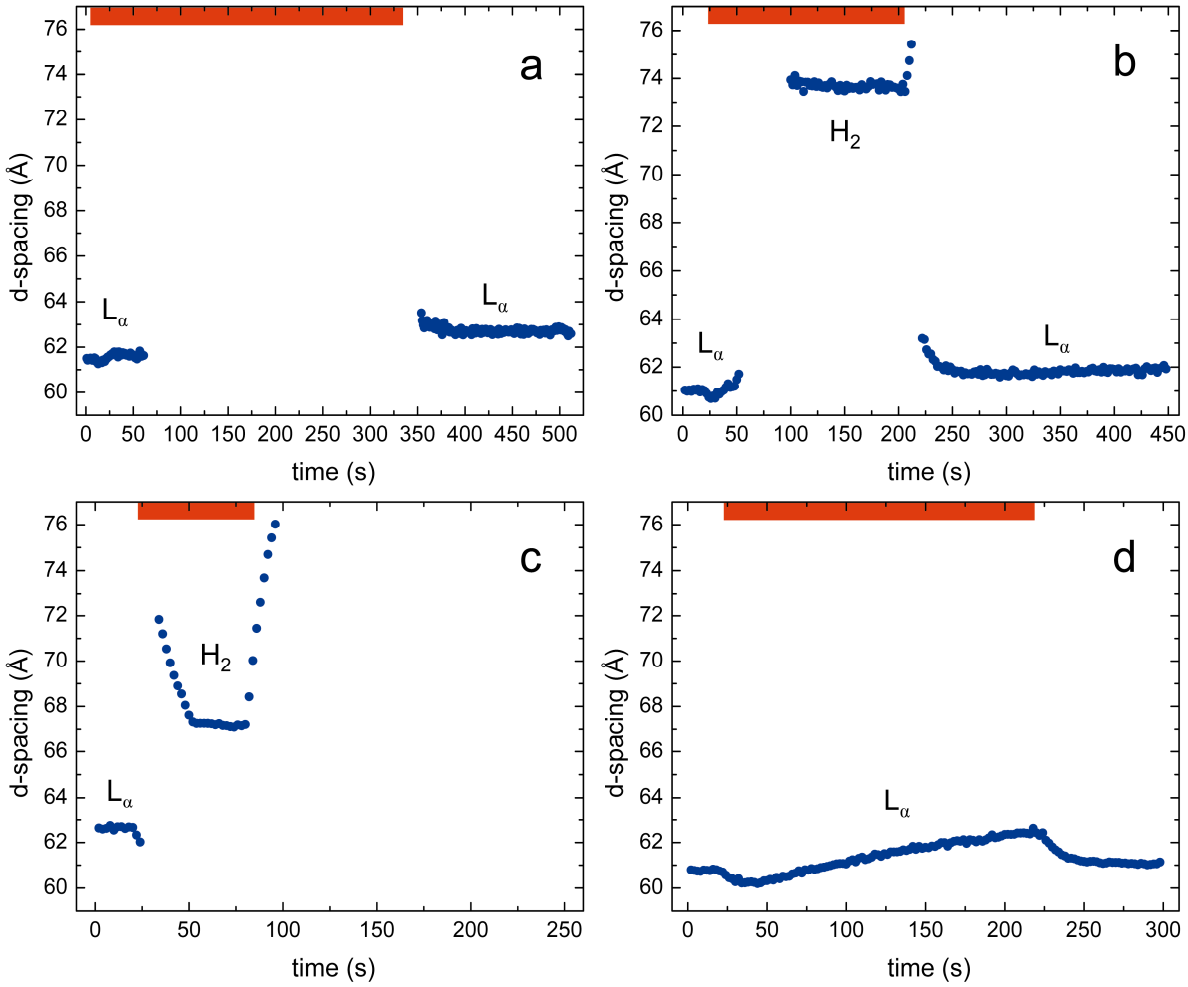

Figure S3. Evolution of the lattice spacings during the time-resolved SAXS experiments on NPs-loaded liposomes (panels a-c refer to Figure 1a-c), and the evolution of a control experiment of unloaded liposomes (d). UV-light heating time is marked with a red bar. While all gold NPs-loaded liposomes display temperature-induced phase transitions, the control sample remains in the fluid L_α phase and displays only a small swelling of about 1 Å during switching on the UV light. This small effect might be due to the used Anton Paar capillary holder, which was to the greatest part shielded from the UV-light, but not completely. Therefore, it could be that its body, which is made of stainless steel, has transmitted a slight conductive heat.

References

(1) Rappolt, M., Hickel, A., Bringezu, F., Lohner, K. *Biophys. J.* **2003**, *84*, 3111–3122.

(2) Warren, B. E. **1969**. X-ray Diffraction. Addison-Wesley, Reading.

(3) Harper, P. E., Mannock, D. A., Lewis, R. N., McElhaney, R. N., Gruner, S. M. *Biophys. J.* **2001**, *81*, 2693–2706.

(4) Pabst, G., Rappolt, M., Amenitsch, H., Laggner, P. *Phys. Rev. E* **2000**, *62*, 4000-4009.

(5) Rappolt, M. In *Advances in Planar Lipid Bilayers and Liposomes*. A. Leitmannova-Liu, Ed., Elsevier: Amsterdam, **2006**; Vol. 5, pp. 253-283.

(6) Paasonen, L.; Laaksonen, T.; Johans, C.; Yliperttula, M.; Konturri, K.; Urtti, A. *J. Controlled Release* **2007**, 122, 86-93.

(7) Gruner, S. M.; Tate, M. W.; Kirk, G. L.; So, P. T. C.; Tunrer, D. C.; Keane, D. T. *Biochemistry* **1988**, *27*, 2853-2866.

(8) Siegel, D. P.; Banschbach, J. L. *Biochemistry* **1990**, *29*, 5975-5981.

(9) Cherezov, V.; Siegel, D. P.; Shaw, W.; Burgess, S. W.; Caffrey, M. *J. Membrane Biol.* **2003**, *195*, 165-182.

(10) Siegel, D. P.; Tenchov, B. G. *Biophys. J.* **2008**, *94*, 3987–3995.

(11) Siegel, D. P.; Cherezov, V.; Greathouse, D. V.; Koeppe, R. E.; Killian, J. A.; Caffrey, M. *Biophys. J.* **2006**, *90*, 200–211.